Progress In Electromagnetics Research C, Vol. 136, 229–244, 2023

A Multi-Layer Metasurface-Enabled Design of Bandpass Filter Screens with Reconfigurable Transmission Bandwidth

Amartya Banerjee[1], Soumya Chakravarty[1], Tapas Chakravarty[1, *], and Rowdra Ghatak[2]

Abstract—In this paper, a novel design concept that uses multi-layer metasurface structures to design and develop bandpass filter screens is proposed. The unique proposition of the work lies in the control of transmission bandwidth of such metasurface screens, which has been obtained by sequential arrangement of unit cell layers, that comprise of Minkowski fractal-shaped unit cells and its complement. This reconfigurability of the structure is achieved without changing the geometry of the unit cell design, rather by stacking the layers in different configurations, or even by changing the substrate thickness, leading to the capability to obtain either narrowband or broadband filtering screens as per the requirement. An equivalent circuit model is proposed to explain such behaviour. Two configurations of stacked complementary surfaces, namely the Patch-Slot-Patch (PSP) and the Slot-Patch-Slot (SPS) designs have been investigated. The PSP structure on a thinner dielectric substrate offered dual band resonance with distinguishable transmission peaks, whereas the same configuration on substrate of increased thickness offered wider transmission bandwidth (45.5% to 50.5% percentage bandwidth). In comparison, the SPS structure offered much narrower transmission bandwidth (varies between 4.7% to 8.16%). The effect of changing the periodicity of the unit cell elements, without altering the fractal unit cell dimensions, has been described, through which one can control the band of operation and roll-off performance of the screens. The simulation results are found to be in good agreement with the measured results of the fabricated prototypes.

1. INTRODUCTION

Filter structures [1] are well known in electronics for their abilities to allow a set of frequencies to pass, while attenuating the others. Well-known filter configurations, such as the Butterworth, Chebyshev, or Elliptic filters, in the form of planar microstrip and transmission line-based designs are widely reported and investigated over the RF range [2, 3]. Also, in recent times, two-dimensional (2D) bandpass transmissive surfaces [4–7], acting as spatial filters of frequencies, have become a rigorously investigated domain. Such structures are widely used in wireless communication systems, radars, radome design technologies [8–10], and lensing applications [11–13] for antenna gain enhancement. Such frequency selective surfaces are now getting modified, with their unit cell elements being replaced by their sub-wavelength counterparts, towards novel outcomes in terms of their transmission and reflection characteristics, leading to a new class of planar 2D structures. Such structures are termed as metasurface, which have introduced a new domain of interest to the researchers.

Metasurface structures are conceived as thin 2D layers of sub-wavelength resonators that can be designed for anomalous electromagnetic (EM) behavior in frequency ranges from microwave to optical [14–16]. The 'unit cells', which are arranged to generate the 2D metasurfaces, can be visualized as sub-wavelength elements where their dimensions are much smaller than the operating wavelength [17–19]. For such, structures like metal patches/slots (in metals) or their combinations [20–22] are used

Received 29 June 2023, Accepted 9 August 2023, Scheduled 21 August 2023
* Corresponding author: Tapas Chakravarty (tapas.chakravarty@tcs.com).
[1] TCS Research, Kolkata, India. [2] National Institute of Technology, Durgapur, India.

to conceive the unit cells for practical requirements. The vast diversity of applications for such metasurface-based structures is highlighted in [23, 24], where suitable unit cells are designed in the optical frequency range to be utilized for reconfigurable transmission and absorption performance. In the articles the notion of reconfigurability is achieved through thermal and electronic means, respectively, which further highlights the immense potential of such meta-unit cell designs for practical operations. Fractal-shaped unit cells are known to offer wideband or multiband performances as transmissive or reflective components, and quite a few of them have gained popularity in metamaterial-based investigations [25, 26]. For bandwidth control and lensing actions pertaining to transmissive metasurfaces, multi-layer stacked configurations are proposed, which offer higher bandwidth and higher phase control for such structures [12, 13].

Multi-layered stacked metasurface designs are analyzed in detail in literature [27], and they are mostly utilized for trasnmitarray systems. These multi-layer structures are used to control both the magnitude of transmission and the corresponding phase for the propagating EM wave. Such control is achieved by judiciously altering the element dimensions [28–30], or by incorporating passive and active components to the design, which consequently makes the design more complex for analysis. The theoretical limits of the obtainable phase difference from such structures are investigated in [27]. Multi-layer frequency selective metasurface designs are proposed and analyzed in [31–33] highlighting their bandpass filtering nature for practical operations. Visualizing the filters as two-port, lossless, reciprocal systems, an analytical approach based on non-normalized resonant modes is proposed in [31] to characterize, design, and establish multi-layer microwave bandpass filter configurations. In [32], regular-shaped unit cell elements such as square patch, square grid, or equivalent slot structures are modeled and analyzed to generate different types of filtering characteristics.

In [31], the authors have reasoned that, to achieve frequency selective characteristics, the array of metallic patches/slots, which provide equivalent capacitive or inductive responses, are used to implement practical LC resonator circuits in RFs. This provides the required bandpass or bandstop characteristics for the developed surfaces. Later, for the analysis of multi-layer configurations, each such layer is modeled separately as equivalent impedance elements, and the substrates in between are modeled as equivalent transmission lines. Likewise, in [31] the authors have presented the design and analysis of second and third order bandpass metasurface structures with multi-layer configuration, suitable for X-band range of operation. The structures provided about 20% percentage bandwidth for all the proposed configurations. The idea of achieving reconfigurability through judiciously choosing constituent layers in the configuration was absent in [31], which on the contrary creates the basic premise for novelty of the work to be presented in this article. In the designs presented in [32], multi-layer unit cells were again visualized as composite constituent units. The reconfigurability of bandwidth performance, by simple alteration of geometric dimensions of the shapes, was not highlighted.

In this article, Minkowski fractal-shaped metallic patches or slots are constructed and incorporated on suitable dielectric substrates to design and develop the multi-layer stacked unit cell elements for suitable transmission characteristics. The elements are later used to implement larger metasurface screens for configurable filtering operation to selectively permit a given frequency set, reducing co-channel interference. A novel design concept of stacking the complementary slot and patch layers on one another, with substrate layers in between, is discussed. The unique idea that by varying the substrate thickness and unit cell periodicities, one can implement a control over the bandwidth of operation, is proposed. Reconfigurability of the structure is achieved without changing the geometry of the unit cell design, rather by stacking different layers in different configurations. This highlights the property of such metasurface designs, where one can maintain a collection of slot or patch-based unit cell array layers, and by arranging them in the required configuration, one can achieve narrowband or wideband filtering functionalities.

An equivalent circuit model is further developed to analyse and explain the behaviour of the designs, where the impinging electromagnetic waves are assumed to be normal to the metasurface. The initial design is conducted through Floquet mode analysis of the unit cell elements using CST Studio Suite^{TM} [34]. Two distinct layer arrangements are then proposed, viz. Slot-Patch-Slot (SPS) and Patch-Slot-Patch (PSP) configurations for characterization. Each of these configurations describes unique transmission properties with varying passband bandwidths and frequencies that can be altered by varying the unit cell periodicity or thickness of the substrate, thus allowing the user better choice

of transmission bandwidth and the concerned roll-off performance. The PSP structure on a thinner dielectric substrate offered dual band resonance with distinguishable transmission peaks, whereas the same configuration on a substrate of increased thickness offered wider transmission bandwidth (45.5% to 50.5% percentage bandwidth). The SPS structure offered much narrower transmission bandwidth of 4.7% to 8.16%, depending on the unit cell periodicity of the configuration. Therefore, this article quantitatively demonstrates that, by changing the substrate thickness or unit cell periodicity values, one can configure the bandwidth of the structures as per requirement, and also alter between narrowband and wideband characteristics by judiciously choosing the constituent layers in the stacked metasurface configurations.

Rest of the paper is arranged as follows. Section 2 of this article will present the design objective followed by the network model representation. Section 3 will include the simulation results and analysis, followed by fabrication and validation of the structures through the measurement in Section 4. Accordingly, the concluding comments and consulted references will be appended.

2. DESIGN FORMULATION AND NETWORK MODEL

The design started with investigating the transmission characteristics of double layer unit cells with Minkowski shaped patch on both sides of the substrate. Later the patch and slot shapes are utilized to envisage simple three-layer unit cell designs for bandpass filtering application. A general transmissive unit cell, which is the basic building block of any frequency selective metasurface, can be visualized as per the schematic shown in Fig. 1(a), where E_{inc}, E_{trs}, and E_{ref} respectively represent the incident, transmitted, and reflected signals. Fig. 1(b) simplifies the representation to a two-port network configuration with the directions of the propagating waves, showing the incident, transmitted, or reflected components as per observation. Multi-layer structures can be visualized as compositions of such two-port networks in a cascaded manner. The said concept is used for detailed scattering analysis of such composite designs. The general relationship between the propagating waves for a general two-port transmissive network is given in (1). From the application perspective, such bandpass transmissive configurations find special use in lensing and gain-enhancing purposes as electromagnetic screens placed in front of primary radiators.

$$\begin{bmatrix} E_1^- \\ E_2^- \end{bmatrix} = \begin{bmatrix} s_{11} & s_{12} \\ s_{21} & s_{122} \end{bmatrix} \begin{bmatrix} E_1^+ \\ E_2^+ \end{bmatrix} \tag{1}$$

In this article, the proposed basic unit cell consists of a metallic fractal structure (or its equivalent complementary fractal slot as etched out from a metal sheet), having a Minkowski fractal geometry, on a layer of suitable dielectric substrate. This geometry is referred to as a Minkowski unit cell henceforth. Minkowski fractal geometry indicates that a square patch has been miniaturized using the Minkowski

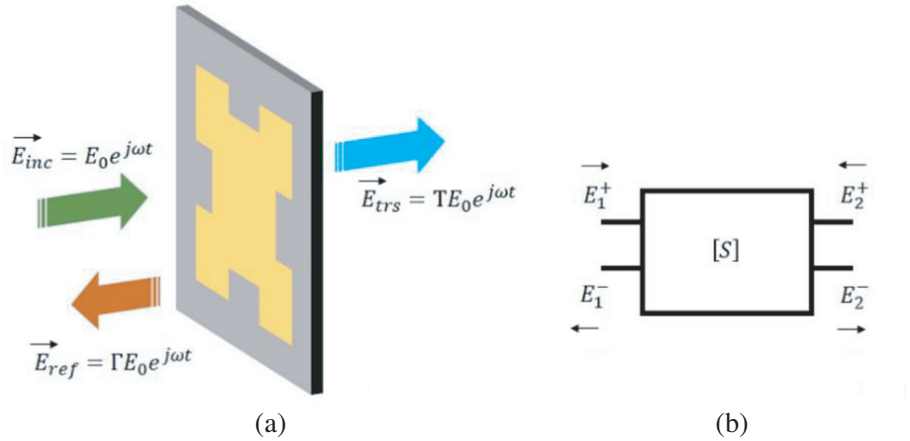

Figure 1. (a) Schematic diagram of a general transmissive unit cell and (b) its two-port network representation.

fractal miniaturization technique to modify and reroute the current flowing path on the metallic patch surface to make the effective path length increase, thus decreasing the resonance frequency without increasing the physical size of the structure. Consequently, the patch size remains confined or constrained within a suitable and specific substrate dimension, and the frequency of resonance is altered by varying the parameters of the fractal operation, which are the indentation depth (d), indentation width (w), and number (N) of iterations of the operator [35]. In all the designs described henceforth in the following sections, only the first iteration of the Minkowski fractal operator has been applied. The designs are simulated using CST Studio Suite^{TM}. For unit-cell simulations Floquet mode analysis technique is used, utilizing the Frequency Domain Solver, with suitable boundary conditions. The open boundaries along the wave propagation path are kept at $\lambda/4$ distance on both sides of the unit cell, with λ being the operating wavelength at the lowest frequency of observation. Later, for simulating the larger array structures, which will represent the actual fabricated prototypes, Time Domain Solver module with Plane Wave excitation in CST is used. The Minkowski patch and slot shapes which are utilized to envisage the multilayer stacked metasurface designs on FR4 substrates ($\varepsilon_r = 4.3$, $\tan\delta = 0.018$), having height h, are described in Fig. 2. On both sides of the substrate, metallic patches or the etched-out slots are implemented of same dimensions, with Minkowski geometry. The proposed unit cells are visualized on dielectric slab layers having periodicity L as shown in Figs. 2 and 3.

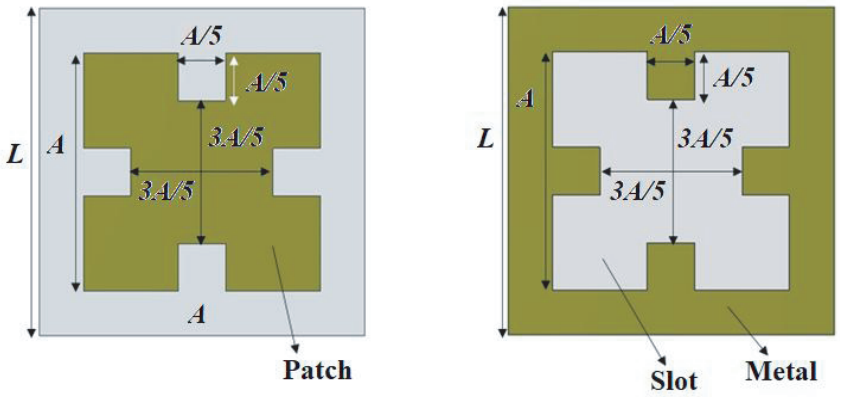

Figure 2. Minkowski unit cell design having periodicity L, for (a) patch and (b) slot configurations.

These unit cell geometries are used to conceive the multilayer stacked metasurface configurations, as shown in Fig. 3, which describes the two-layer Patch-Substrate-Patch configuration along with the three-layer Patch-Slot-Patch (PSP) and Slot-Patch-Slot (SPS) configurations, printed and stacked on substrate layers of height h and predefined unit cell periodicity L respectively.

A general multi-layered configuration with dielectric slabs in between can be envisaged as a ladder network as shown in Fig. 4, where the substrate layers are modelled as transmission lines of equivalent length. Each layer of patch, slot, or substrate is considered as a constituent element having specific network parameters; the networks are cascaded to offer the composite transmissive behaviour of the structure.

Each constituent element of this network can be represented by an $ABCD$ matrix. Thus, the overall $[ABCD]$ matrix of the network represented by Fig. 4 is given in (2),

$$[ABCD_{composite}] = [ABCD_{patch(slot)}] \times [ABCD_{dielectric}] \times [ABCD_{slot(patch)}] \times [ABCD_{dielectric}] \times [ABCD_{patch(slot)}] \quad (2)$$

The patch or slot layers can be modelled accordingly in terms of their surface impedance values, which are calculated when the incident beam is directed normally to the surface [32],

$$Z^{TE}_{patch} = -j\frac{\eta_{eff}}{2\alpha} \quad (3)$$

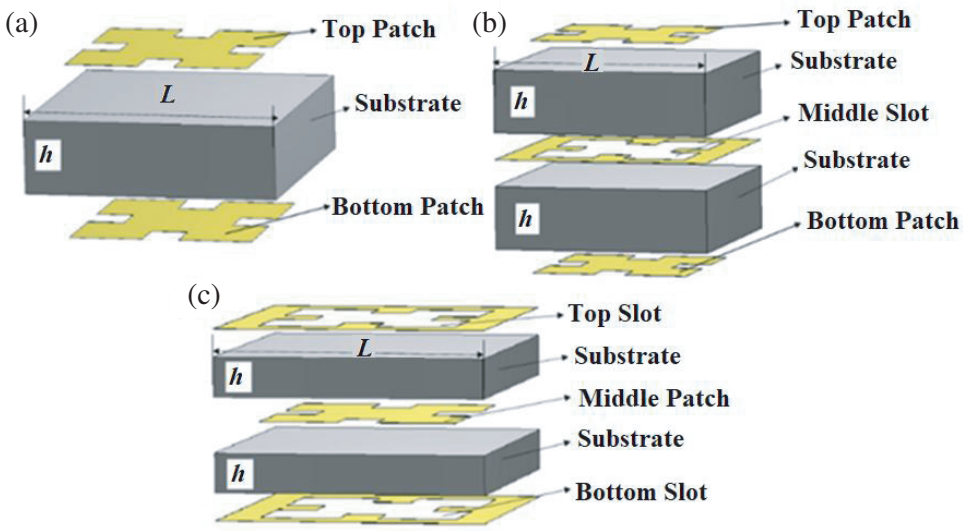

Figure 3. Exploded view of (a) two-layer Patch-Patch and three-layer, (b) Patch-Slot-Patch (PSP), (c) Slot-Patch-Slot (SPS) configurations.

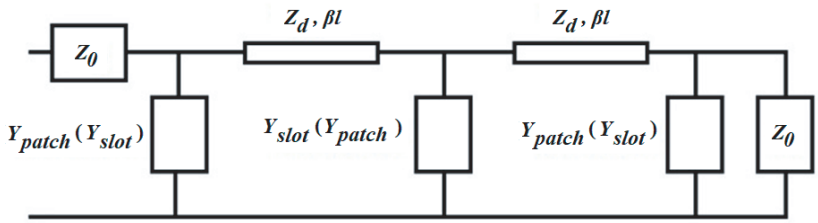

Figure 4. Equivalent ladder network representation for multilayer stacked metasurface configurations.

$$Z_{slot}^{TE} = j\frac{\eta_{eff}\,\alpha}{2} \tag{4}$$

$$\eta_{eff} = \frac{Z_0}{\sqrt{\varepsilon_{eff}}} \tag{5}$$

where,

$$\varepsilon_{eff} = \frac{\varepsilon_r + 1}{2} + \frac{\varepsilon_r - 1}{2}\left[1 + 12\frac{h}{W}\right]^{-\frac{1}{2}} \tag{6}$$

W is the width of the metallic strip on substrate and Z_0 = free-space impedance = $377\,\Omega$.

In [32], the value of $Z_{patch(slot)}$ so obtained is converted to $ABCD$ matrix as given below,

$$\left[ABCD_{patch(slot)}\right] = \begin{bmatrix} 1 & 0 \\ Y_{patch(slot)} & 1 \end{bmatrix} \tag{7}$$

where $Y_{patch(slot)} = \frac{1}{Z_{patch(slot)}}$.

However, the intrinsic impedances given by (3) and (4) are at best termed as quasi-static approximations of a Minkowski shaped patch on a thin dielectric slab. The alternate approach is to conduct a Floquet port simulation of the patch (or slot) on an electrically thin dielectric slab where the unit-cell periodicity is also considered. From the S-parameters, thus obtained, $ABCD$ matrix values are extracted using the following equations [36],

$$A = \frac{\left(Z_{01}^{*} + S_{11}Z_{01}\right)\left(1 - S_{22}\right) + S_{12}S_{21}Z_{01}}{2S_{21}\sqrt{R_{01}R_{02}}} \tag{8a}$$

$$B = \frac{(Z_{01}^{*} + S_{11}Z_{01})(Z_{02}^{*} + S_{22}Z_{02}) - S_{12}S_{21}Z_{01}Z_{02}}{2S_{21}\sqrt{R_{01}R_{02}}} \tag{8b}$$

$$C = \frac{(1 - S_{11})(1 - S_{22}) - S_{12}S_{21}}{2S_{21}\sqrt{R_{01}R_{02}}} \tag{8c}$$

$$D = \frac{(1 - S_{11})(Z_{02}^{*} + S_{22}Z_{02}) - S_{12}S_{21}Z_{02}}{2S_{21}\sqrt{R_{01}R_{02}}} \tag{8d}$$

where, * indicates the complex conjugate, Z_{0j} the normalized impedance for the j^{th} port of the system, and R_{0j} the real part of the normalized impedance for the j^{th} port.

In (8), the impedance values of Z_{0j} are represented by Equations (3) and (4) for patch and slot, respectively. For the present article the port impedances at both the ports of the envisaged two port networks are considered as equal, i.e., $Z_{01} = Z_{02}$ for (8). In [32], α is defined only for square patch and corresponding slot. Also, in [33] the authors have outlined that major inaccuracies in such models result from "near-field coupling between layers". Taking the cue from such observations, in this work α is empirically introduced as a proportionality constant acting as a correction factor for Minkowski shape which depends on periodicity L of the unit-cell and height h of the substrate material.

Dielectric substrate layers having impedance Z_d and electrical length βl can be modeled as equivalent transmission lines having network parameters as,

$$[ABCD_{dielectric}] = \begin{bmatrix} \cos\beta l & jZ_d \sin\beta l \\ \dfrac{1}{Z_d}\sin\beta l & \cos\beta l \end{bmatrix} \tag{9}$$

Z_d for a dielectric slab having dielectric constant $= \varepsilon_r$ is calculated as,

$$Z_d = \frac{Z_0}{\sqrt{\varepsilon_{eff}(1 - j\tan\delta)}} \tag{10}$$

Therefore, the ladder network depicted in Fig. 4 can now be visualized as if five individual layers (viz. the patch (slot), the substrate, the slot (patch), the substrate and the patch (slot)), each having specific $ABCD$ network parameters, are cascaded together, and consequently the composite $ABCD$ network parameters for the entire configuration are obtained using Equation (2). The overall response obtained as $[ABCD_{composite}]$ is now converted back into S-parameters using (11) which are then compared with simulation results.

$$S_{11} = \frac{AZ_{02} + B - CZ_{01}^{*}Z_{02} - DZ_{01}^{*}}{AZ_{02} + B + CZ_{01}Z_{02} + DZ_{01}} \tag{11a}$$

$$S_{21} = \frac{2(AD - BC)\sqrt{R_{01}R_{02}}}{AZ_{02} + B + CZ_{01}Z_{02} + DZ_{01}} \tag{11b}$$

where $Z_{01} = Z_{02} = Z_0 =$ free-space impedance $= 377\,\Omega$.

To validate the approach described as above, a double-layer Patch-Substrate-Patch configuration, as shown in Fig. 3(a), is modelled. Fig. 5(a) represents the equivalent circuit, and Fig. 5(b) represents the comparison between simulation results and equivalent circuit model. The graphs show a good agreement, highlighting the low-pass nature of the configuration. It is seen that at low enough frequency of 1 GHz (quasi-static case), the Minkowski patch is represented by equivalent capacitance of 0.023 pF, whereas the corresponding slot is represented by equivalent inductance 0.59 nH.

3. STACKED THREE-LAYER TRANSMISSIVE METASURFACE SIMULATIONS

While simulating the three-layer Patch-Slot-Patch (PSP) configuration as described in Fig. 3(b), the configuration is investigated with two different substrate thickness values to observe its effect on the transmission performance. The software used for electromagnetic simulations is CST Studio Suite™. In Fig. 6, the S-parameter plots are presented for different unit cell periodicity values at a substrate thickness of $h = 0.8$ mm (as described in Fig. 3(b)). Both the images in Fig. 6 depict dual resonance transmission characteristics with slight frequency shifts happening due to the change in L. When

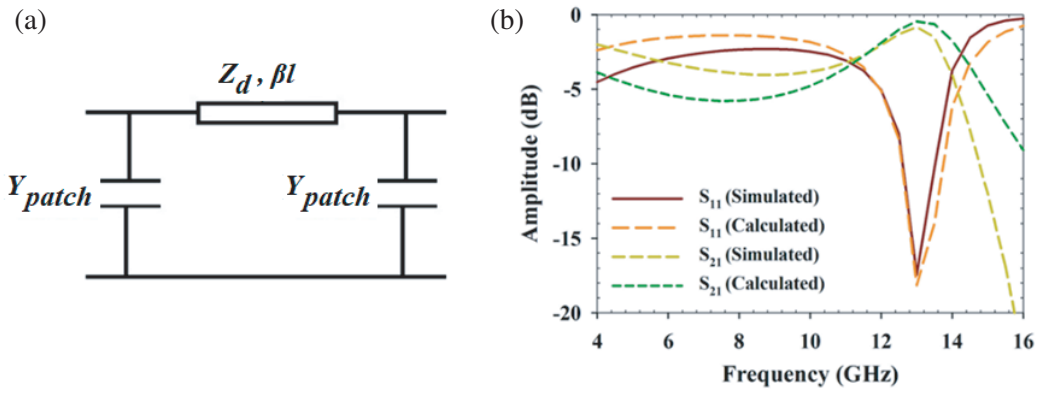

Figure 5. (a) Equivalent circuit model of the Patch-Substrate-Patch configuration shown in Fig. 3, and (b) comparison between the theoretical and simulated S-parameter results, for $A = 4\,\text{mm}$, $L = 5.5\,\text{mm}$, and $h = 1.6\,\text{mm}$ respectively.

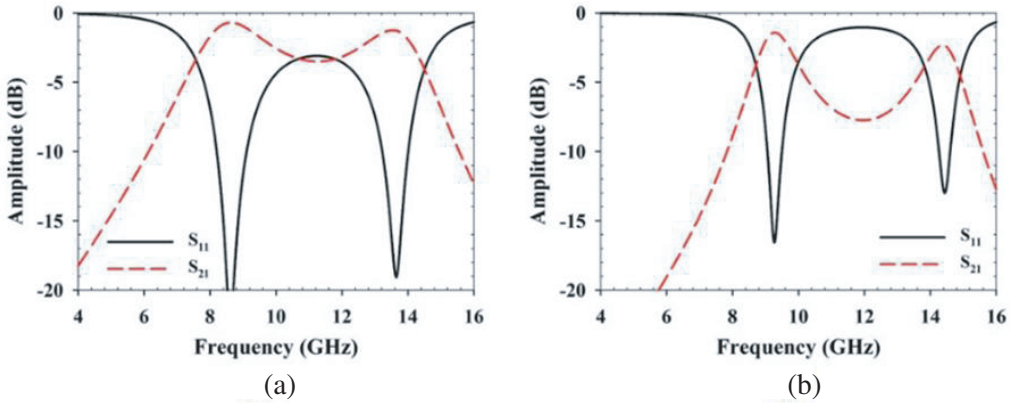

Figure 6. Simulated reflection and transmission characteristics for the unit cell with the PSP configuration; $h = 0.8\,\text{mm}$, $A = 4\,\text{mm}$ and (a) $L = 5.5$, (b) $L = 8\,\text{mm}$.

$L = 5.5\,\text{mm}$, the first and second resonance points are observed at 8.61 GHz and 13.53 GHz, respectively, and when the value of L is increased to 8 mm, the two resonance points are shifted to 9.35 GHz and 14.41 GHz. Ratios between the first and second resonance frequency points are observed to be 0.63 and 0.65 for $L = 5.5\,\text{mm}$ and 8 mm, respectively. When the substrate thickness is increased to a value of $h = 1.6\,\text{mm}$ (as described in Fig. 3(b)), a wideband transmission characteristic is obtained from these configurations (as shown in Fig. 7) with the $-3\,\text{dB}$ bandwidth ranging from 7.16 GHz to 12 GHz, for a total bandwidth of 4.84 GHz, when $L = 5.5\,\text{mm}$. This bandwidth covers the entire X-band (8–12 GHz). Thus, this structure acts as a wideband bandpass filter that can be tuned to allow only certain frequencies. On increasing the value of L to 8 mm (Fig. 7(b)), the wideband response shifts to higher frequencies with the $-3\,\text{dB}$ bandwidth ranging from 8.83 GHz to 14.03 GHz (total 5.2 GHz bandwidth). Therefore, for $L = 5.5\,\text{mm}$ and 8 mm, the configurations on a thicker substrate offer nearly flat wideband transmission performance with percentage bandwidth values of 50.5% and 45.5%, respectively.

This three-layer PSP configuration can now be described in the form of an equivalent circuit model as shown in Fig. 8. The same figure also represents the comparison between the theoretically calculated S-parameter values with those of the simulations (calculated at unit cell periodicity value of $L = 5.5\,\text{mm}$, $A = 4\,\text{mm}$, $h = 1.6\,\text{mm}$), which shows good agreement, highlighting the bandpass nature of the configuration. The S-parameter results of the composite network model are obtained by calculating the layer-by-layer $ABCD$ parameter values and consequently cascading them to realize the composite configuration, as described in the previous section.

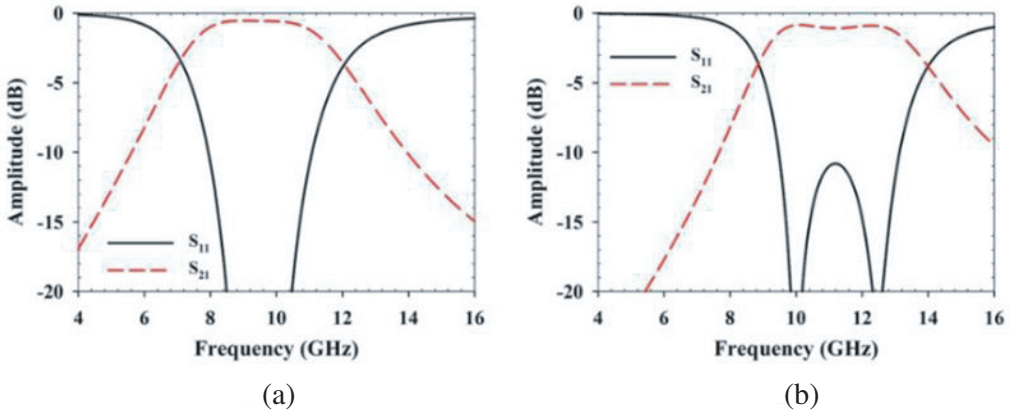

Figure 7. Simulated reflection and transmission characteristics for the unit cell with the PSP configuration; $h = 1.6\,\text{mm}$, $A = 4\,\text{mm}$ and (a) $L = 5.5\,\text{mm}$, (b) $L = 8\,\text{mm}$.

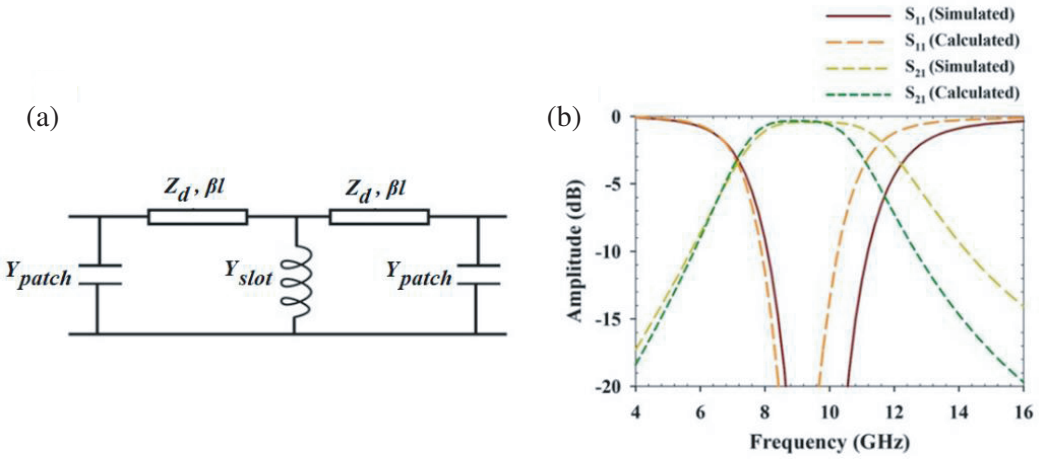

Figure 8. (a) Equivalent circuit model of the Patch-Slot-Patch (PSP) configuration and (b) comparison between the theoretical and simulated S-parameter results calculated at unit cell periodicity of $L = 5.5\,\text{mm}$, $A = 4\,\text{mm}$, $h = 1.6\,\text{mm}$.

The Slot-Patch-Slot (SPS) configuration (as described in Fig. 3(c)) is now investigated. In Fig. 9, the simulated reflection and transmission characteristics of the unit cell, with $A = 4\,\text{mm}$ and $h = 0.8\,\text{mm}$, are shown. It is observed from Fig. 9(a) that there is only one transmission peak (and one corresponding resonance dip) at 9.85 GHz, when $L = 5.5\,\text{mm}$. This transmission is happening over a very narrow bandwidth, from 9.45 GHz to 10.25 GHz (about 800 MHz bandwidth, percentage bandwidth = 8.16%). On increasing L to 8 mm (Fig. 9(b)), the transmission peak shifts to 10 GHz, but transmission bandwidth is narrowed even further to 470 MHz (percentage bandwidth = 4.7%). The roll-off bandwidth in Fig. 9(a) is also higher (8.52 GHz) than that in Fig. 9(b), where the roll-off bandwidth is 4.34 GHz.

Such a three-layer SPS configuration can also be represented in the form of an equivalent circuit model as shown in Fig. 10(a). Fig. 10(b) shows the comparison between the theoretically calculated S-parameter values and those of the simulations (calculated at unit cell periodicity value of $L = 5.5\,\text{mm}$, $A = 4\,\text{mm}$, $h = 0.8\,\text{mm}$), which shows a good agreement, highlighting the bandpass nature of the configuration. The S-parameter results of the composite network model are obtained by calculating the layer-by-layer $ABCD$ parameters and consequently cascading them to realize the composite configuration, as described in the previous section.

According to Figs. 8 and 10, it can be observed that slight variations are present between the simulated and equivalent circuit model results, for both the Patch-Slot-Patch (PSP) and Slot-Patch-

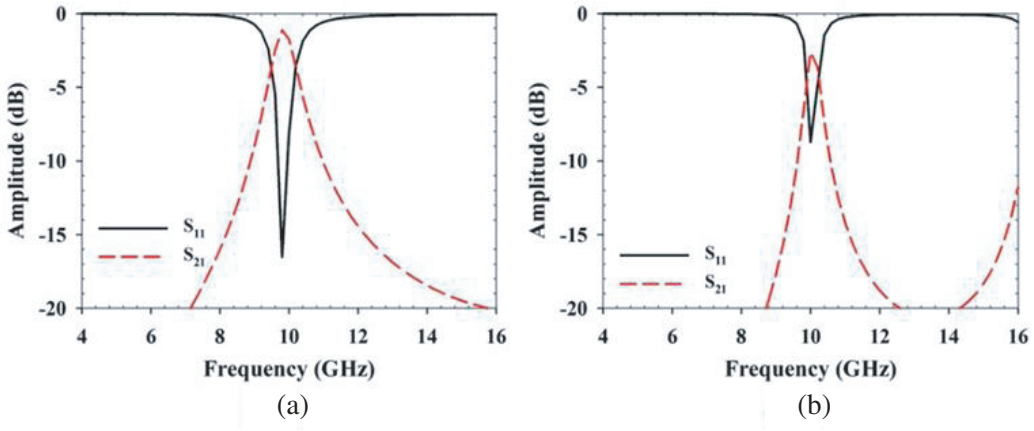

Figure 9. Simulated reflection and transmission characteristics for the unit cell with the SPS configuration; $h = 0.8\,\text{mm}$, $A = 4\,\text{mm}$ and (a) $L = 5.5\,\text{mm}$, (b) $L = 8\,\text{mm}$.

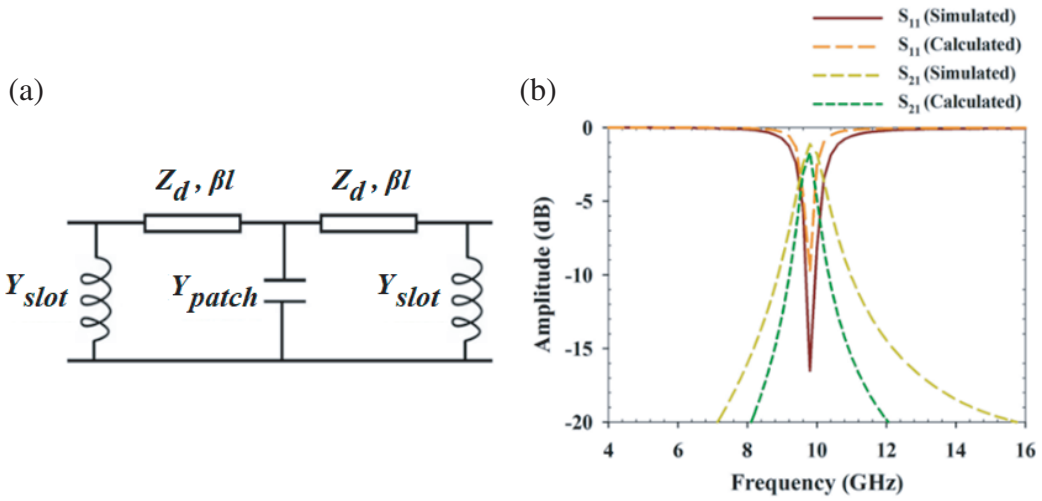

Figure 10. (a) Equivalent circuit model of the Slot-Patch-Slot (SPS) configuration and (b) comparison between the theoretical and simulated S-parameter results calculated at unit cell periodicity of $L = 5.5\,\text{mm}$, $A = 4\,\text{mm}$, $h = 0.8\,\text{mm}$.

Slot (SPS) configurations. The discrepancy increases as one moves to the higher frequency regions. In [33], the authors have outlined that major inaccuracies from such equivalent models result from "near-field coupling between layers". For higher frequency regions the effect of near field coupling increases. However, the observations recorded provide a benchmark for further analysis.

The designed unit cells are now investigated for their oblique incidence performance and both the Patch-Slot-Patch (PSP) and Slot-Patch-Slot (SPS) structures described stable transmission and reflection characteristics for angle of incidence values going up to 30 degrees in simulations. For higher values of angle of incidence, the magnitude performance gradually deteriorated; however the characteristic curves retained their transmissive/reflective nature and shape till 35 to 40 degrees. Figs. 11(a)–(b) describe the oblique incidence characterization results for the PSP and SPS structures, respectively, which quantitatively justify the claims.

Table 1 quantitatively describes the passband bandwidth ($-3\,\text{dB}$ bandwidth) and roll-off performance ($-20\,\text{dB}$ bandwidth) parameters for the SPS configurations, which decisively confirms that by judiciously determining the periodicity of the designs, one can control the transmission bandwidth and concerned roll-off performance for such bandpass frequency selective metasurfaces. In Table 1, the

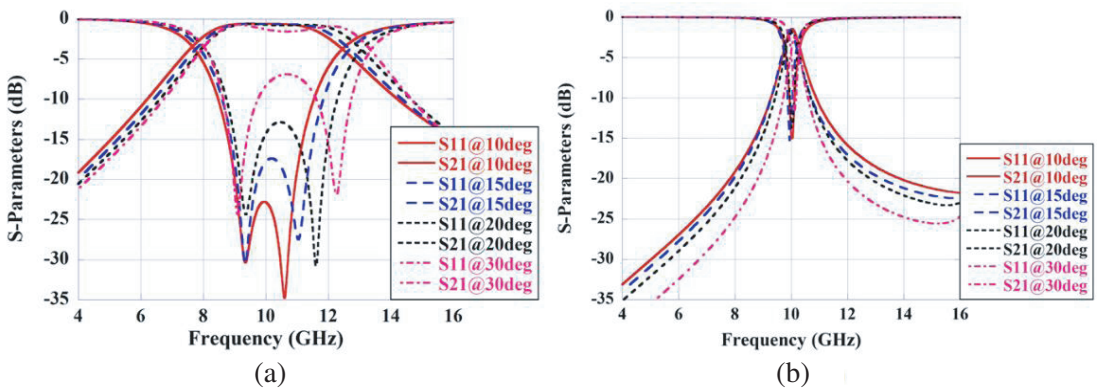

Figure 11. Oblique incidence performance for the (a) PSP (unit cell periodicity = 5.5 mm, substrate thickness = 1.6 mm) and (b) SPS (unit cell periodicity = 5.5 mm, substrate thickness = 0.8 mm) configurations respectively.

Table 1. Transmission and roll-off bandwidth (−20 dB) performance for SPS configurations.

L (mm)	h (mm)	Centre Frequency (GHz)	−3 dB Transmission Bandwidth (T_x) (GHz)	Percentage Bandwidth	−20 dB Roll-off Bandwidth (R_o) (GHz)	Ratio (R_o/T_x)
5.5	0.8	9.85	0.8	8.16%	8.52	10.65
8	0.8	10	0.47	4.7%	4.34	9.23

ratio of the roll-off and transmission bandwidths are calculated, which gives an estimate of the filter order of the narrowband bandpass filter configurations. With the increase in L, while keeping the value of h constant, the ratio decreases, implying that the filter response slope is gradually becoming steeper, which consequently allows the user a control over it by means of changing the appropriate parameter.

The next section presents arrays of such unit meta cells to study the response of the surface to an impinging electromagnetic wave.

4. SIMULATION AND EXPERIMENTAL VALIDATION OF THE METASURFACE RESPONSE TO AN INCIDENT ELECTROMAGNETIC WAVE

Arrays with the following specifications were considered for numerical simulation as well as experimental validation of the transmission and reflection characteristics of the metasurface.

i. An array consisting of 20×20 periodic arrangement of the SPS configuration unit cell with $A = 4$ mm and $h = 0.8$ mm for each substrate layer, for two values of L — 5.5 mm and 8 mm.
ii. An array consisting of 20 × 20 periodic arrangement of the PSP configuration unit cell with $A = 4$ mm and $h = 1.6$ mm for each substrate layer, for two values of L — 5.5 mm and 8 mm.

Figures 12(a)–(e) describe different simulation views for E-field propagation at 9.85 GHz (which is the center passband frequency for the SPS configuration, as per simulation) for the Slot-Patch-Slot configuration and at 10.45 GHz (which is out of band for the same). Here, the 20 × 20 SPS array structure is investigated with a plane wave excitation. From Figs. 12(b)–(e), which represent the different cut-planes of E-field propagation, it is evident that at 9.85 GHz the incident wave excites the metasurface with noticeable field convergence on the plane of incidence, and the wave is gradually transmitted through the plates on the other side. On the other hand, at 10.45 GHz, similar field convergence is absent at the plane of incidence, and the transmitted wave is significantly attenuated,

establishing the stopband characteristics. Moreover, in Figs. 12(b), (d), during passband transmission, field convergence of the transmitted wave suggests a focusing nature, which consequently opens up the prospect of further ideas and investigations. The SPS configuration is narrowband in nature, and this plane wave simulation is exclusively carried out for the same, to quantitatively highlight the passband and stopband phenomenon. Similar characteristics can be established for the PSP structure as well.

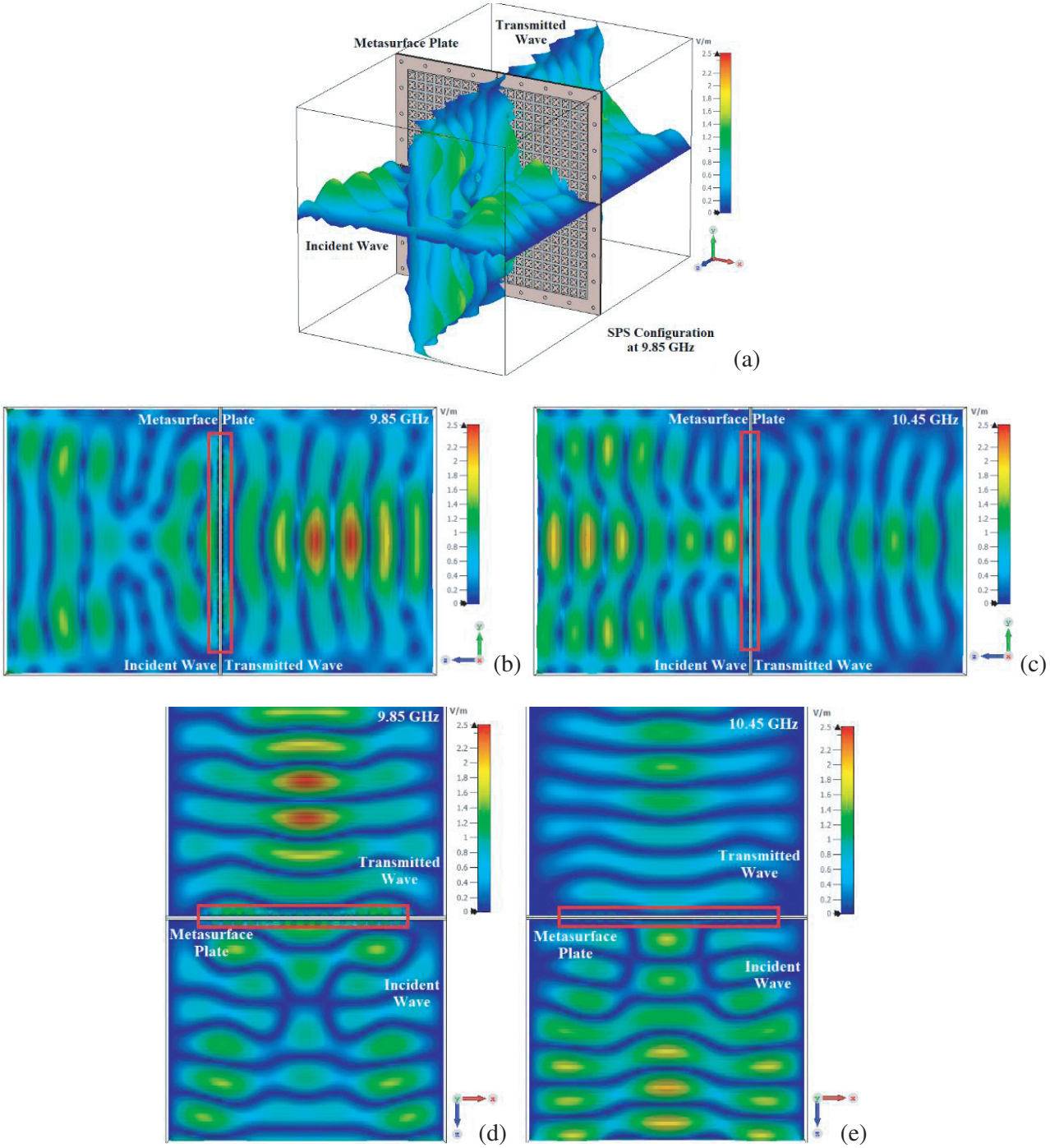

Figure 12. (a) Perspective view of the simulation setup with the metasurface being excited by a plane wave source, (b) E-field propagation along YZ plane at 9.85 GHz and (c) 10.45 GHz, (d) E-field propagation along XZ plane at 9.85 GHz and (e) 10.45 GHz.

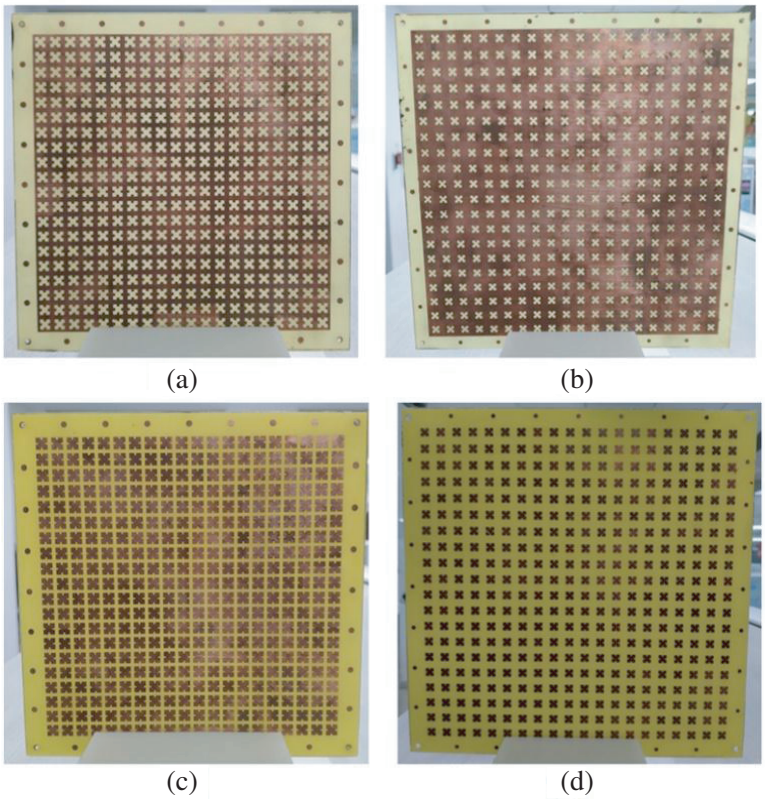

Figure 13. 20×20 arrangement of the unit cells: (a) slot array layer for $L = 5.5\,\text{mm}$, (b) slot array layer for $L = 8\,\text{mm}$, (c) patch array layer for $L = 5.5\,\text{mm}$ and (d) patch array layer for $L = 8\,\text{mm}$.

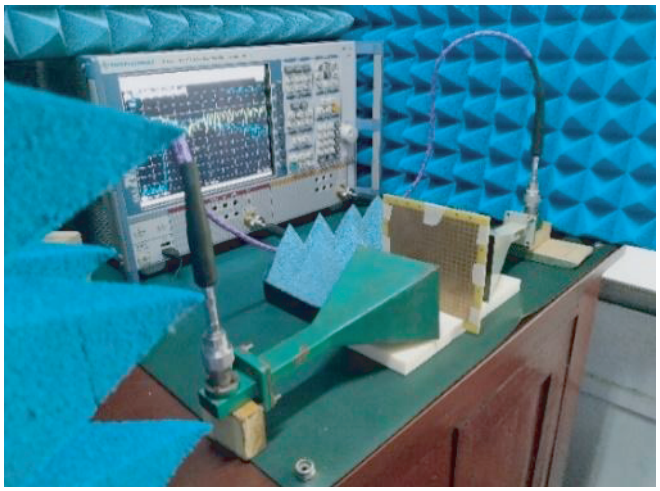

Figure 14. Setup diagram with the VNA and the standard gain horn antennas, which were used for characterizing the fabricated transmission metasurfaces.

Photographs of the fabricated prototypes with $L = 5.5\,\text{mm}$ and $8\,\text{mm}$ are shown below in Fig. 13. There are several circular markings at the edges of each array structure, which indicate places where holes were drilled for aligning the two substrates and connecting them with Teflon posts.

The configurations are measured using two identical standard gain X-band standard gain horn antennas fed by WR90 waveguide to coaxial adapters. The S-parameters were measured using Vector

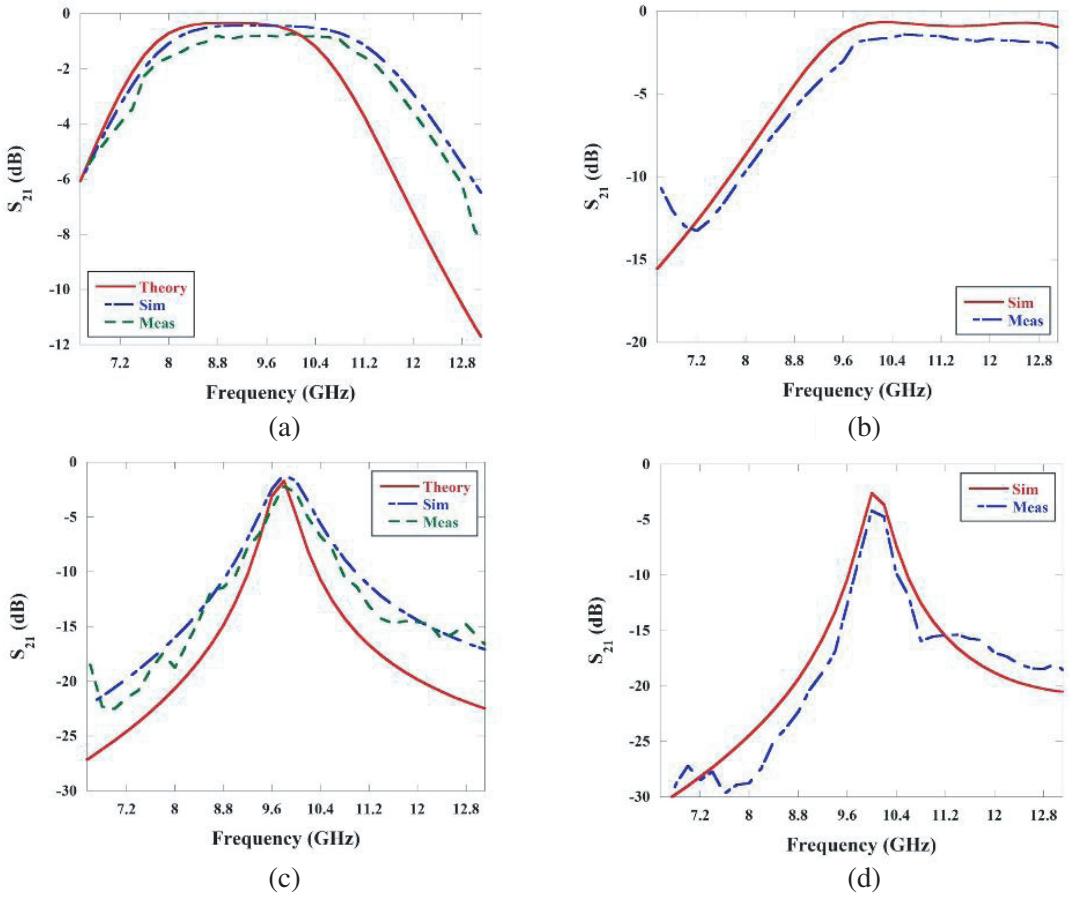

Figure 15. Result comparison for the fabricated prototypes viz. (a) PSP (unit cell periodicity = 5.5 mm, substrate thickness = 1.6 mm), (b) PSP (unit cell periodicity = 8 mm, substrate thickness = 1.6 mm), (c) SPS (unit cell periodicity = 5.5 mm, substrate thickness = 0.8 mm) and (d) SPS (unit cell periodicity = 8 mm, substrate thickness = 0.8 mm) configurations against theory and simulations.

Table 2. Comparison of performance for the contributed work in this article, with recent literature.

Reference Number	Percentage Bandwidth Obtained	Reconfigurability Technique
[31]	1.1% to 11.7%	Filter orders are changed, Number of layers are varied in the unit cell design
[37]	31% (prototype value)	Filter orders are to be changed to attain reconfigurability
[38]	34.4% to 53%	Through mechanical re-positioning of the components
[39]	Bandwidth can be tuned between 6.07 GHz to 6.61 GHz	Through electronic control by using lumped varactor components
Present Work	**4.7% to 50.5%**	**Through judicious choice of constituent layers in the multi-layer unit cell design**

Network Analyzer (ZVA40, Rohde and Schwarz) under minimal ambient reflection conditions. Fig. 14 describes the experimental setup used for measurements. Figs. 15(a)–(d) compare the measured results for each of the surfaces against the simulation results and theoretical predictions, where they clearly depict sound agreement with the measurements.

A collection of recent literature is presented in Table 2, compared to the present article, which aims to quantitatively justify the contributions of the latter and highlights the technique of configuring bandwidth performance by judiciously choosing the constituent layers of a multi-layer unit cell design, which is proposed in this work for such bandpass surfaces.

5. CONCLUSION

In this article, Minkowski fractal-shaped metallic patches or slots are constructed and incorporated on suitable dielectric substrates to design and implement larger metasurface screens for configurable filtering operation. Such structures are suitable to selectively permit a given frequency set, reducing co-channel interference under practical considerations. An equivalent circuit model is proposed to analyze and explain the behaviour of the filter screens, where the impinging electromagnetic waves are assumed to be normal to the metasurface. The proposed configurations describe unique transmission properties with varying passband bandwidths and frequencies that can be altered by varying the unit cell periodicity or thickness of the substrate, thus allowing the user's better choice of transmission bandwidth and the concerned roll-off performance. Reconfigurability of the structure is achieved without changing the geometry of the unit cell design, rather by stacking the different complementary layers in different configurations. The two configurations proposed in this article, namely the Patch-Slot-Patch (PSP) and Slot-Patch-Slot (SPS) multi-layer configurations with Minkowski shaped transmissive elements, are shown to offer controllable passband bandwidths, and the work quantitatively demonstrates that by changing the substrate thickness or unit cell periodicity values, one can configure the bandwidth of the structures as per requirement. One can also alter between narrowband and wideband characteristics by judiciously choosing the constituent layers in the stacked metasurface configurations. Measured results for the prototypes agree well with the simulations and theoretical predictions.

REFERENCES

1. Dimopoulos, H. G., *Analog Electronic Filters: Theory, Design and Synthesis*, Springer Science & Business Media, Dordrecht, Netherlands, 2011.
2. Levy, R., *Classic Works in RF Engineering: Volume-2-Microwave and RF Filters*, Artech House, MA, USA, 2007.
3. Tang, C. W. and M. G. Chen, "A microstrip ultra-wideband bandpass filter with cascaded broadband bandpass and bandstop filters," *IEEE Transactions on Microwave Theory and Techniques*, Vol. 55, No. 11, 2412–2418, 2007.
4. Sarabandi, K. and N. Behdad, "A frequency selective surface with miniaturized elements," *IEEE Transactions on Antennas and Propagation*, Vol. 55, No. 5, 1239–1245, 2007.
5. Munk, B. A., *Frequency Selective Surfaces: Theory and Design*, John Wiley & Sons, New York, NY, 2005, ISBN: 978-0-471-37047-5.
6. Bayatpur, F. and K. Sarabandi, "Single-layer high-order miniaturized-element frequency-selective surfaces," *IEEE Transactions on Microwave Theory and Techniques*, Vol. 56, No. 4, 774–781, 2008.
7. Huang, H. F. and H. Huang, "Millimeter-wave wideband high effeciency circular airy OAM multibeams with multiplexing OAM modes based on transmission metasurfaces," *Progress In Electromagnetic Research*, Vol. 173, 151–159, 2022.
8. Foroozesh, A. and L. Shafai, "Investigation into the effects of the patch-type FSS superstrate on the high-gain cavity resonance antenna design," *IEEE Transactions on Antennas and Propagation*, Vol. 58, No. 2, 258–270, 2010.
9. Chiu, C. N. and K. P. Chang, "A novel miniaturized-element frequency selective surface having a stable resonance," *IEEE Antennas and Wireless Propagation Letters*, Vol. 8, 1175–1177, 2008.

10. Wu, T.-K., *Frequency Selective Surface and Grid Array*, Wiley-Interscience, 1995, ISBN: 978-0471311898.
11. Li, H. P., G. M. Wang, J. G. Liang, and X. J. Gao, "Wideband multifunctional metasurface for polarization conversion and gain enhancement," *Progress In Electromagnetic Research*, Vol. 155, 115–125, 2016.
12. Al-Joumayly, M. A. and N. Behdad, "Wideband planar microwave lenses using sub-wavelength spatial phase shifters," *IEEE Transactions on Antennas and Propagation*, Vol. 59, No. 12, 4542–4552, 2011.
13. Li, M., M. A. Al-Joumayly, and N. Behdad, "Broadband true time-delay microwave lenses based on miniaturized element frequency selective surfaces," *IEEE Transactions on Antennas and Propagation*, Vol. 61, No. 3, 1166–1179, 2013.
14. Yu, N. and F. Capasso, "Flat optics with designer metasurfaces," *Nature Materials*, Vol. 13, 139–150, 2014.
15. Ding, F., A. Pors, and S. I. Bozhevolnyi, "Gradient metasurfaces: A review of fundamentals and applications," *Reports on Progress in Physics*, Vol. 81, 2018, DOI: 10.1088/1361-6633/aa8732.
16. Chen, M., M. Kim, A. M. H. Wong, and G. V. Eleftheriades, "Huygens' Metasurfaces from microwaves to optics: A review," *Nanophotonics*, Vol. 7, 1207–1231, 2018.
17. Caloz, C. and T. Itoh, *Electromagnetic Metamaterials: Transmission Line Theory and Microwave Applications*, Wiley Interscience, John Wiley & Sons, 2006, ISBN 978-0-471-66985-2.
18. Epstein, A. and G. V. Eleftheriades, "Huygens' metasurfaces via the equivalence principle: Design and applications," *Journal of the Optical Society of America B*, Vol. 33, No. 2, A31–A50, 2016.
19. Joseph, P., S. Wong, M. Selvanayagam, and G. V. Eleftheriades, "Design of unit cells and demonstration of methods for synthesizing huygens metasurfaces," *Photonics and Nanostructures: Fundamentals and Applications*, Vol. 12, No. 4, 360–375, 2014.
20. Lavigne, G., K. Achouri, V. S. Asadchy, S. A. Tretyakov, and C. Caloz, "Susceptibility derivation and experimental demonstration of refracting metasurfaces without spurious diffraction," *IEEE Transactions on Antennas and Propagation*, Vol. 66, No. 3, 1321–1330, 2018.
21. Capolino, F., A. Vallecchi, and M. Albani, "Equivalent transmission line model with a lumped X-circuit for a metalayer made of pairs of planar conductors," *IEEE Transactions on Antennas and Propagation*, Vol. 61, No. 2, 852–861, 2013.
22. Rabinovich, O. and A. Epstein, "Analytical design of Printed-Circuit-Board (PCB) metagratings for perfect anomalous reflection," *IEEE Transactions on Antennas and Propagation*, Vol. 66, No. 8, 4086–4095, 2018.
23. Hadi Badri, S., H. Soofi, and S. SaeidNahaei, "Thermally reconfigurable extraordinary terahertz transmission using vanadium dioxide," *Journal of the Optical Society of America B*, Vol. 39, No. 6, 1614–1621, 2022.
24. Hadi Badri, S., M. M. Gilarlue, S. SaeidNahaei, and J. S. Kim, "Narrowband-to-broadband switchable and polarization-insensitive terahertz metasurface absorber enabled by phase-change material," *Journal of Optics*, Vol. 24, No. 2, 2022, DOI: 10.1088/2040-8986/ac3c50.
25. Bengin, V. C., V. Radonic, and B. Jokanovic, "Fractal geometries of complementary split-ring resonators," *IEEE Transactions on Microwave Theory and Techniques*, Vol. 56, No. 10, 2312–2321, 2008.
26. Moeini, S., "Homogenization of fractal metasurface based on extension of Babinet-Booker's principle," *IEEE Antennas and Wireless Propagation Letters*, Vol. 18, No. 5, 1061–1065, 2019.
27. Abdelrahman, A. H., F. Yang, A. Z. Elsherbeni, and P. Nayeri, *Analysis and Design of Transmitarray Antennas*, Morgan & Claypool, 2017, ISBN: 9781627058742.
28. Abdelrahman, A. H., F. Yang, and A. Z. Elsherbeni, "Transmission phase limit of multilayer frequency selective surfaces for transmitarray designs," *IEEE Transactions on Antennas and Propagation*, Vol. 62, No. 2, 690–697, 2014.

29. Ryan, C. G. M., M. Reza, J. Shaker, J. R. Bray, Y. M. M. Antar, and A. Ittipiboon, "A wideband transmitarray using dual-resonant double square rings," *IEEE Transactions on Antennas and Propagation*, Vol. 58, No. 5, 1486–1493, 2010.
30. Milne, R., "Dipole array lens antenna," *IEEE Transactions on Antennas and Propagation*, Vol. 30, No. 4, 704–712, 1982.
31. Benzaouia, M., J. D. Joannopoulos, S. G. Johnson, and A. Karalis, "Analytical criteria for designing multiresonance filters in scattering systems, with application to microwave metasurfaces," *Physical Review Applied*, Vol. 17, No. 3, 2022, DOI: https://doi.org/10.1103/PhysRevApplied.17.034018
32. Xu, Y. and M. He, "Design of multilayer frequency-selective surfaces by equivalent circuit method and basic building blocks," *International Journal of Antennas and Propagation*, Vol. 2019, Article ID 9582564, 13 pages, 2019, DOI: 10.1155/2019/9582564.
33. Olk, A. E. and D. A. Powell, "Accurate metasurface synthesis incorporating near field coupling effects," *Physical Review Applied*, Vol. 11, 2019, DOI: 10.1103/PhysRevApplied.11.064007.
34. https://www.3ds.com/products-services/simulia/products/cst-studio-suite/.
35. Manafi, S. and H. Deng, "Design of a small modified minkowski fractal antenna for passive deep brain stimulation implants," *International Journal of Antennas and Propagation*, Vol. 2014, No. 12, Article ID 749043, 9 pages, 2014, DOI: https://doi.org/10.1155/2014/749043.
36. Freaky, D. A., "Conversions between S, Z, Y, h, $ABCD$ and T parameters which are valid for complex source and load impedances," *IEEE Transactions on Microwave Theory and Techniques*, Vol. 42, No. 2, 205–211, 1994.
37. Lalbakhsh, A., M. U. Afzal, K. P. Esselle, and S. L. Smith, "All-metal wideband frequency-selective surface bandpass filter for TE and TM polarizations," *IEEE Transactions on Antennas and Propagation*, Vol. 70, No. 4, 2790–2800, 2022
38. Qiu, S., Q. Guo, and Z. Li, "Tunable frequency selective surface based on a sliding 3D-printed inserted dielectric," *IEEE Access*, Vo. 9, 19743–19748, 2021.
39. Jin, C., Q. Lv, B. Zhang, J. Liu, S. An, Z. S. He, and Z. Shen, "Ultra-wide-angle bandpass frequency selective surface," *IEEE Transactions on Antennas and Propagation*, Vol. 69, No. 9, 5673–5681, 2021.